Monthly Notices
of the
ROYAL ASTRONOMICAL SOCIETY

MNRAS **491,** 2706–2714 (2020)
Advance Access publication 2019 November 15

doi:10.1093/mnras/stz3197

Determination of the star-spot covering fraction as a function of stellar age from observational data

Fiona Nichols-Fleming [1,2]★ and Eric G. Blackman[2,3]★

[1]*Department of Earth, Environmental and Planetary Sciences, Brown University, Providence, RI 02912, USA*
[2]*Department of Physics and Astronomy, University of Rochester, Rochester, NY 14627, USA*
[3]*Laboratory for Laser Energetics, University of Rochester, Rochester, NY 14623, USA*

Accepted 2019 November 12. Received 2019 October 23; in original form 2019 September 6

ABSTRACT

The association of star-spots with magnetic fields leads to an expectation that quantities which correlate with magnetic field strength may also correlate with star-spot coverage. Since younger stars spin faster and are more magnetically active, assessing whether star-spot coverage correlates with shorter rotation periods and stellar youth tests these principles. Here, we analyse the star-spot covering fraction versus stellar age for M-, G-, K-, and F-type stars based on previously determined variability and rotation periods of over 30 000 *Kepler* main-sequence stars. We determine the correlation between age and variability using single and dual power-law best fits. We find that star-spot coverage does indeed decrease with age. Only when the data are binned in an effort to remove the effects of activity cycles of individual stars, do statistically significant power-law fits emerge for each stellar type. Using bin averages, we then find that the star-spot covering fraction scales with the X-ray to bolometric ratio to the power λ with $0.22 \pm 0.03 < \lambda < 0.32 \pm 0.09$ for G-type stars of rotation period below 15 d and for the full range of F- and M-type stars. For K-type stars, we find two branches of λ separated by variability bins, with the lower branch showing nearly constant star-spot coverage and the upper branch $\lambda \sim 0.35 \pm 0.04$. G-type stars with periods longer than 15 d exhibit a transition to steeper power law of $\lambda \sim 2.4 \pm 1.0$. The potential connection to previous rotation-age measurements suggesting a magnetic breaking transition at the solar age, corresponding to period of 24.5 is also of interest.

Key words: stars: activity – stars: evolution – stars: magnetic field – stars: solar-type – starspots – X-rays: stars.

1 INTRODUCTION

During the Sun's 11-yr activity cycle, dark sunspots appear for time-scales ranging from days to a few months (Petrovay & van Driel-Gesztelyi 1997). The appearance and disappearance of these sunspots produce brightness variations on different time-scales, which can be detected in total solar irradiance (TSI) data (e.g. Domingo et al. 2009). Stars other than the Sun also have activity cycles and variations in chromospheric emission (Wilson 1978; Vaughan & Preston 1980; Noyes et al. 1984; Noyes, Weiss & Vaughan 1984). These variations are typically measured with the S index, which is based on the Ca II H and K lines (Vaughan, Preston & Wilson 1978), but can also be observed with long-term brightness variations (Baliunas & Vaughan 1985; Oláh, Kolláth & Strassmeier 2000; Messina & Guinan 2002; Oláh & Strassmeier 2002).

Baliunas et al. (1995) found a separation in mean values of S indices for fast- and slow-rotating main-sequence stars which have higher and lower S values, respectively, indicating that younger stars exhibit more activity than older stars. Additionally, two distinct branches have been identified in the relation between rotation and dynamo cycle period, which have been labelled the active (A) and inactive (I) sequences, where the inactive branch applies to slower rotators and has rotation to dynamo cycle period ratios about six times larger than the active branch. (Brandenburg, Saar & Turpin 1998; Saar & Brandenburg 1999). There is also a separate branch for fast rotators with rotation periods less than 3 d. The A and I branches were confirmed by Böhm-Vitense (2007) who also saw the Sun placed between the two branches, but evidence for these multiple branches has not been robustly confirmed by the more recent study of do Nascimento, Saar & Anthony (2015).

Indicators of stellar activity are believed to be driven by the stellar magnetic dynamo (Parker 1955; Wilson 1966; Kraft 1967; Charbonneau 2014), which is in turn thought to be driven by some combination of convection, rotation, and differential rotation

★ E-mail: fiona_nichols-fleming@brown.edu (FN-F); blackman@pas.rochester.edu (EGB)

(Duvall et al. 1984). Given this correlation, the dynamo dependence on rotation for slow rotators like the Sun suggests that an overall decrease in indicators of stellar activity over much longer timescales should correlate with spin-down of the stars driven by their stellar winds (e.g. Skumanich 1972; Pizzolato et al. 2003; Mamajek & Hillenbrand 2008). The stellar winds likely depend on energy sources that strengthen with magnetic field and the magnetic dynamo (Cranmer & Saar 2011), and therefore these correlations create a positive feedback loop (e.g. Blackman & Owen 2016).

Large sample observations allow extraction of empirical scalings of coronal activity versus rotation period or Rossby number (*Ro*), where *Ro* is the ratio of rotation period to a stellar model-dependent eddy turnover time (Wright et al. 2011; Reiners, Schüssler & Passegger 2014). Wright et al. (2011) show that for older main-sequence stars with $Ro > 0.13$, the ratio of the X-ray to bolometric flux of the star, used as a metric of activity, varies as $Ro^{-\zeta}$ where $2 \leq \zeta \leq 3$. For younger main-sequence stars with $Ro < 0.13$, the relationship saturates. Reiners et al. (2014) emphasize that the eddy turnover time is itself luminosity dependent and so favours relations directly scaling activity to rotation period. For present purposes, we ignore stars in the saturated regime as the population has multivalued periods for a given luminosity and because we exclude stars so young that accretion is still influencing their behaviour.

Since star-spot coverage and X-ray luminosity are both closely related to the stellar magnetic dynamo, we may expect a relationship between star-spot coverage and rotation period of stars, and therefore between star-spot coverage and the ratio of X-ray to bolometric flux of the star. Notsu et al. (2019) found that star-spot area does not depend on rotation period for young stars, but begins to decrease quickly for rotation periods greater than about 12 d for Sun-like stars. This observed trend is based on chromospheric lines, so further investigation of the trend based on photometric brightness is timely.

There have been some previous efforts to characterize star-spot coverage from photometric brightness variations measured by the *Kepler Space Telescope* (Dmitrienko & Savanov 2017; Savanov & Dmitrienko 2017a,b; Savanov & Dmitrienko 2018). These authors measure star-spot coverage of various samples of main-sequence stars, with an S factor based on changes in the mean radiation flux of the stars. Savanov & Dmitrienko (2017a) found two groups of solar-type stars, active and inactive, based on the stars' S values. The active group is only about 10 per cent of the sample, but has a mean S value about the same as that of the Sun. The active sample has a decreasing trend in S value with age while the inactive sample has a constant S value. Dmitrienko & Savanov (2017) look at the relationship between S values for M dwarfs and Rossby numbers and find that it resembles that found in Wright et al. (2011) with saturation at the same value of *Ro*. Although these works identify a decreasing trend in star-spot coverage as stars age, further efforts to identify a functional form of this relationship are warranted and to assess whether there is evidence for any dynamo transitions that have been purported for solar-type stars in smaller samples (van Saders et al. 2016; Metcalfe & van Saders 2017).

In Section 2, we discuss the theoretical connection between stellar age, X-ray luminosity, and rotation. In Section 3, we discuss the observational sample used in this work. In Section 4, we discuss our analysis methods. In Section 5, we present our results for single and dual power-law relationships as well as trends in vertically binned data. In Section 6, we discuss the theoretical implications of this work. We conclude in Section 7.

2 CONNECTING STELLAR ACTIVITY, AGE, ROTATION, AND STAR-SPOT COVERAGE

Different theoretical or semitheoretical approaches have been pursued to understand aspects of the observed relationship between coronal activity and rotation period (Pallavicini et al. 1981; Noyes et al. 1984; Vilhu 1984; Micela et al. 1985; Hartmann & Noyes 1987; Randich 2000; Montesinos et al. 2001; Pizzolato et al. 2003; Wright et al. 2011; Reiners et al. 2014; Vidotto et al. 2014; Blackman & Thomas 2015). To highlight the role of star-spot covering fraction in this effort, note for example the work of Blackman & Thomas (2015) in which they connected the activity evolution over stellar spin-down times to saturation of a dynamo model for fast rotators. In doing so, the authors parametrized a relation between the ratio of X-ray to bolometric luminosity ratio $\frac{\mathcal{L}_X}{\mathcal{L}_*}$ and the solid angle that the magnetic field passes through, Θ of the form

$$\Theta = \Theta_0 \left(\frac{\mathcal{L}_X/\mathcal{L}_*}{6.6 \times 10^{-7}} \right)^{\lambda}, \tag{1}$$

where Θ_0 is the cycle averaged value of Θ for the present Sun, and λ is a needed parameter to account for the decreasing star-spot coverage fraction with age discussed further below. This work also provides an expression for the ratio of X-ray to bolometric luminosity with dependence

$$\frac{\mathcal{L}_X}{\mathcal{L}_*} \propto \left(\frac{s^{1/3}}{1 + 2\pi s\ Ro} \right)^2 \Theta, \tag{2}$$

based on the magnetic energy flux sourced by the internal dynamo that buoyantly rises into the corona, and averaged over a dynamo cycle period. Here s is a constant that accounts for differential rotation in the models of Blackman & Thomas (2015) and *Ro* is the Rossby number. From equations (1) and (2)

$$\frac{\mathcal{L}_X}{\mathcal{L}_*} \propto \left(6.6 \times 10^{-7}\right)^{-\lambda/1-\lambda} \Theta_0^{1/1-\lambda} \left(\frac{s^{1/3}}{1 + 2\pi s\ Ro} \right)^{2/(1-\lambda)} \tag{3}$$

which, when removing the constants from the proportionality, gives

$$\frac{\mathcal{L}_X}{\mathcal{L}_*} \propto \left(\frac{s^{1/3}}{1 + 2\pi s\ Ro} \right)^{2/(1-\lambda)}. \tag{4}$$

For $Ro \gg 1$ and a chosen value of λ, equation (4) can provide a value for ζ, the parameter describing the relationship between Rossby number and X-ray to bolometric flux from Wright et al. (2011). If $\lambda = 0$, then $\zeta \sim 2$ whereas if $\lambda > \frac{1}{3}$, then $\zeta > 3$. As observations have shown that $2 \leq \zeta \leq 3$ (Wright et al. 2011), an empirical value of $0 \leq \lambda \leq \frac{1}{3}$ would be expected. The scaling relation of equation (4) was also used in a subsequent minimalist unified theory for the evolution of X-ray luminosity, rotation, magnetic fields, and mass-loss of main-sequence stars in the unsaturated regime (Blackman & Owen 2016). Direct constraints on λ are timely not only for use in such holistic theoretical approaches, but also as a fundamental observational constraint to be explained from first principles.

3 OBSERVATIONAL SAMPLE

McQuillan, Mazeh & Aigrain (2014) derived rotation periods and measured the photometric variability of 34 030 main-sequence stars based on 3 yr of *Kepler* observations. Rotation periods are found with an autocorrelation method that has been shown to be more robust than the more common Fourier methods (McQuillan, Aigrain & Mazeh 2013). The value of a star's variability is

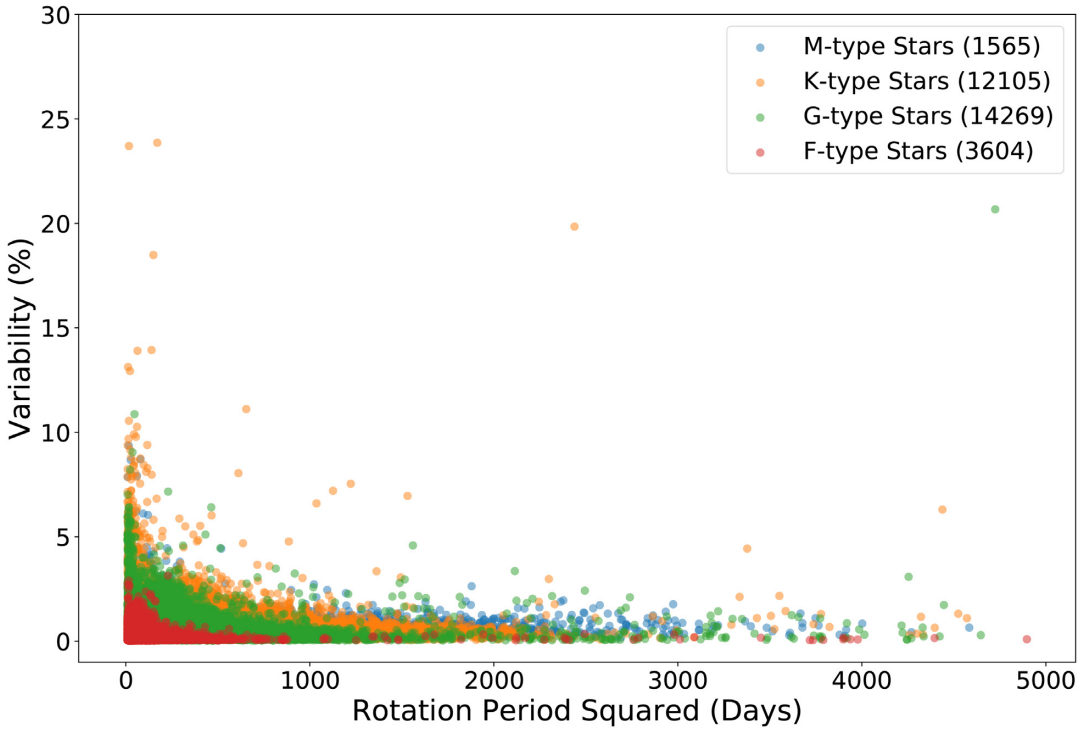

Figure 1. Variability versus rotation period squared for the entire sample of 31 543 stars with rotation periods above 3 d from McQuillan et al. (2014). Rotation period squared is used as a proxy for age where larger P^2 is older, so this plot demonstrates the evolution of stellar activity with age for main-sequence stars. The sample is divided into stellar types based on their effective temperatures and are shown here in different colours: blue for M-type, orange for K-type, green for G-type, and red for F-type. The number of stars for each stellar type is shown in the upper right corner.

defined as the difference between the 95th and 5th percentile of the normalized flux for the star in a single rotation period, then averaged over all rotation periods contained over the duration of the observations.

We do not consider the 2487 stars in the sample with rotation periods shorter than 3 d. These stars were removed due to the risk of ongoing accretion affecting variability, leaving a data set of 31 543 stars. When looking at the 2487 fast rotators, there is indeed a large amount of variability indicating that there is no evidence for a saturated regime in this sample that is not masked by the highly variable regime. McQuillan et al. (2014) also provide stellar parameters for the sample from either the *Kepler* Input Catalog (KIC) or Dressing & Charbonneau (2013), including mass and effective temperature. The sample covers masses $0.256 \leq M/M_{\odot} \leq 1.28$ and effective temperatures 3204 K $\leq T \leq$ 6499 K.

Stars of different types may evolve differently, so we use the effective temperatures to divide the sample into stellar type subgroups using the temperature ranges from Drilling & Landolt (2000). From this we find that we have 3604 F-type stars ($5940 < T \leq 7300$), 14 269 G-type stars ($5150 < T \leq 5940$), 12 105 K-type stars ($3840 < T \leq 5150$), and 1565 M-type stars ($3170 < T \leq 3840$). The variability versus rotation period squared (P^2) for the entire sample is shown in Fig. 1 with colours indicating each star's spectral type and it can be seen that all spectral types have decreasing variability, interpreted as spot coverage, with increasing rotation period (or age). Although the G- and K-type subgroup sizes are the largest, even the samples of F- and M-type stars are still much larger than those of most previous works, and comparable to those of Savanov & Dmitrienko (2017a,b), Dmitrienko & Savanov (2017), and Savanov & Dmitrienko (2018).

4 METHODS

In this work, we assume that the star-spot coverage fraction is directly proportional to the average variability of the star. This may not be valid for all variability regimes, in part because stars may have a certain amount of continuous star-spot coverage. But this is presently hard to account for, so we proceed with this assumption of proportionality for now. Blackman & Thomas (2015) explain that the fraction of the solid angle that the field rises through on its journey to the corona is plausibly proportional to the areal fraction of star-spots and therefore stellar variability can give a measure of the solid angle through which the field rises. Skumanich's 'law' states that the rotation period of a star is approximately proportional to the square root of its age (Skumanich 1972), so we look for a relationship between the variability of the star and its rotation period squared to represent the star-spot coverage evolution in time. To quantify this relationship between star-spot coverage fraction and age, we determine the correlation of these quantities and then attempt to fit the observations with single and dual power laws.

Specifically, we determine the correlation of the data using a Pearson correlation coefficient on the logarithmic relationship between the rotation period squared and the average variability the stars. The Pearson correlation coefficient is defined as

$$r_{P,V} = \frac{\mathrm{cov}(P, V)}{\sigma_P \sigma_V}, \tag{5}$$

where cov(P, V) is the covariance of P^2 and the variability V, and σ_P and σ_V are the standard deviations of P^2 and the variability V, respectively.

We also quantify the statistical significance of our best-fitting functions using a reduced chi-square value. The reduced chi square

is given by

$$\chi^2 = \frac{1}{N-n}\sum_i^N \frac{(V_i - f(P_i))^2}{\sigma_i^2}, \tag{6}$$

where N is the number of data points, n is the number of fit parameters, V_i is the variability value from the data for a given P^2, $f(P_i)$ is the best-fitting value for a given P^2, and σ_i is the variance at a given P^2. To be statistically significant, this reduced χ^2 value should be close to one.

As another way to quantify the change in star-spot covering fraction with age, we determine values of the free parameter λ used in the holistic model of stellar activity evolution of Blackman & Owen (2016) for each stellar type subsample. From equation (1), we find the following expression for λ.

$$\lambda = \frac{\frac{\mathrm{d}}{\mathrm{d}t}\ell n\,(\Theta)}{\frac{\mathrm{d}}{\mathrm{d}t}\ell n\,(\mathcal{L}_\mathrm{X}/\mathcal{L}_*)}. \tag{7}$$

To determine an expression for the ratio of X-ray to bolometric luminosity of a star as a function of its age t, we use the results from Wright et al. (2011)

$$\frac{\mathcal{L}_\mathrm{x}}{\mathcal{L}_*} = C * Ro^\beta \tag{8}$$

where $\beta \equiv -\zeta = -2.70 \pm 0.13$, in combination with Skumanich's law. The Rossby number is proportional to the rotation period divided by the eddy turnover time, and the age is proportional to the rotation period squared. Thus if we assume that the eddy turnover time is constant for a particular stellar type, we find that $Ro \propto P \propto t^{1/2}$ and obtain

$$\frac{\mathcal{L}_\mathrm{x}}{\mathcal{L}_*} = C * t^\alpha, \tag{9}$$

where $\alpha = \frac{1}{2}\beta = -1.35 \pm 0.065$. Equation (9) and the assumption that $\Theta \propto$ Variability $\propto (P^2)^b$ where b is the derived power of our fit, allows us to write our expression for λ (equation 7) in the simpler form[1]

$$\lambda = \frac{b}{\alpha}. \tag{10}$$

To find the error in our values of λ, we use the basic error propagation formula

$$\sigma_f^2 = \sum_{i=1}^N \left(\frac{\mathrm{d}f}{\mathrm{d}x_i}\right)^2 \sigma_{xi}^2, \tag{11}$$

which reduces to

$$\sigma_\lambda^2 = \left(\frac{b}{\alpha^2}\right)^2 \sigma_\alpha^2 + \left(\frac{1}{\alpha}\right)^2 \sigma_b^2, \tag{12}$$

where σ_α is the derived error in α from Wright et al. (2011) and σ_b is the derived error in the power of an individual best-fitting power law found in this work.

For the dual power-law fits, we again look at the Pearson correlation coefficients, reduced χ^2 values, and values of λ for the different age regimes. We look at the Pearson r value for all stars with periods longer and shorter than a chosen transition period and define the formula

$$F_T \equiv 1 - \mathrm{abs}(r_\mathrm{low})\frac{n_\mathrm{low}}{N} - \mathrm{abs}(r_\mathrm{high})\left(1 - \frac{n_\mathrm{low}}{N}\right), \tag{13}$$

where r_low and r_high are the Pearson r values for the points less than and greater than or equal to the transition rotation period recalculated with each transition period choice, respectively; n_low is the number of stars with rotation periods below the transition, and N is the total number of stars of that stellar type. Minimizing F_T of equation (13) with respect to n_low allows us to look for a transition that maximizes the correlations, since the value of n_low is determined by the choice of transition period. For values of λ, we still use equations (10) and (12), but find individual values for each age regime of the dual power law.

Stars at different points in their respective stellar activity cycles likely have different levels of spottiness for a particular age, producing a spread in the variability for stars at a given rotation period. To mitigate this, we employ vertical bins of constant width in variability of 0.1 per cent. This width is based on the observed change in variability of the Sun between solar activity cycle maxima and minima from over 40 yr of observations shown in Reinhold, Cameron & Gizon (2017), and empirical correlations between X-ray and bolometric variability (Preminger, Chapman & Cookson 2011). The general trends do not change significantly with different bin sizes. Each bin is then represented by a single point at the mean of the data within the bin and is given a weight of the fraction of stars in that stellar type. Trends in this binned data again do not change significantly when using the median instead of the mean as shown in Appendix. We again quantify the statistical significance of resulting fits using the reduced chi-square values from equation (6).

5 RESULTS

5.1 Single power law

We first investigate the relationships between the square of the rotation period and the stellar variability informed by the Pearson correlation coefficient analysis. If the relationship were described by a power law, there would be a linear trend in log–log space that can be quantified with the Pearson correlation coefficient. We find Pearson r values of −0.55 for M-type stars, −0.58 for K-type stars, −0.40 for G-type stars, and −0.19 for F-type stars. These all indicate a decreasing relationship between the two parameters, although those of the M-, K-, and G-type stars indicate this more strongly than that of F-type stars.

We characterize the decreasing variability with a single power law of the form Ax^b for each stellar type. We use a Levenberg–Marquardt (LM) minimization routine which returns best-fitting parameters and errors on those derived parameters based on the gradient of the steepest descent in the minimization routine. We find the best fits (shown in Fig. 2):

M-type stars: $(11.72 \pm 0.56)x^{(-0.40 \pm 0.009)}$, $\chi^2 = 64$
K-type stars: $(11.55 \pm 0.31)x^{(-0.43 \pm 0.005)}$, $\chi^2 = 393$
G-type stars: $(3.72 \pm 0.09)x^{(-0.30 \pm 0.005)}$, $\chi^2 = 516$
F-type stars: $(0.65 \pm 0.04)x^{(-0.17 \pm 0.017)}$, $\chi^2 = 124$

We find that our best fits for a single function had very large reduced χ^2 values. None of these values are statistically significant, which suggests that a single power law is not the best function to represent the evolution of activity for any of these stellar types, and we therefore attempt to fit the data with two power laws.

[1] An alternative approach is to use the results of Reiners et al. (2014) where the ratio of X-ray to bolometric luminosity is a function of rotation period and radius rather than the Rossby number. Presently, we restrict ourselves to using the expression from Wright et al. (2011).

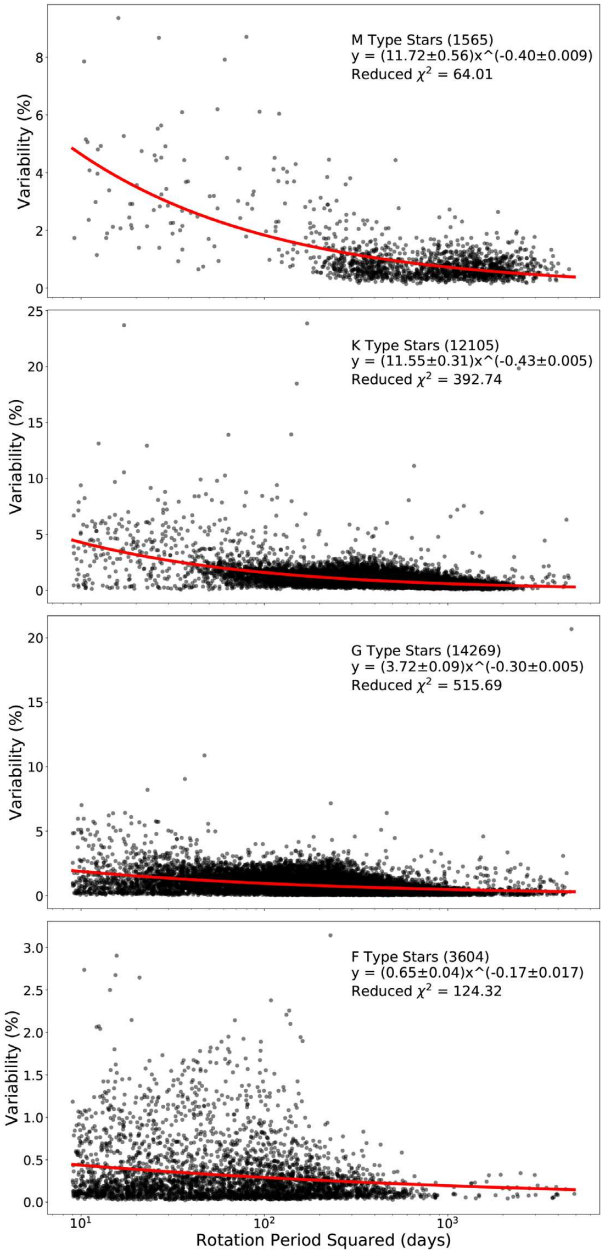

Figure 2. Variability versus rotation period squared with a single power-law fit for each stellar type. The red line on each panel represents the best fit for each stellar type. The particulars of the fits, along with the reduced χ^2 values are labelled on the plot for each stellar type.

5.2 Dual power law

Previous work has suggested there is a change in magnetic field geometry near the age of the Sun for Sun-like main-sequence stars (van Saders et al. 2016). This, and the large reduced χ^2 values from our single power-law fits, prompted us to try to fit the data set with two different power laws. Rather than bias the choice of a possible power-law break to the current solar rotation period, we minimize equation (13), in order to maximize the Pearson correlation to assess whether any of the stellar types show evidence of a dual power law when the break value is determined by the best fit. Our minimization routine for unbinned data finds no significant global minimum of the function for any of the stellar type groups so we

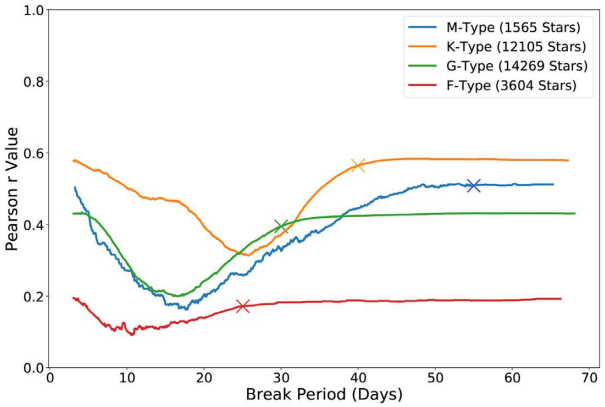

Figure 3. Pearson r values versus break period for each stellar type, blue for M-type stars, orange for K-type stars, green for G-type stars, and red for F-type stars. Each line has an x of the same colour which shows the selected break period for that stellar type. The number of stars for each stellar type is shown in the upper right corner.

are left to a somewhat arbitrary choice. Fig. 3 shows the weighted correlation coefficients for each stellar type along with our choice for the periods at the power-law break. These 'break periods' were simply selected as the points where the curves levelled off after the large minimum in correlation and are 55, 40, 30, and 25 d for M-, K-, G- and F-type stars, respectively. We chose these points as they are the lowest break periods that provide the maximum weighted correlation, allowing for the highest number of stars for the fits of each power law.

Once break periods for each stellar type were selected, we fit each with the LM minimization routine from Section 5.1, but with two power laws that apply for stars with rotation periods less than or greater than the break period, respectively. We find the best fits (shown in Fig. 4):

M-type stars: $(11.79 \pm 0.56)x^{(-0.40 \pm 0.009)}$ for $P_{\rm rot} < 55$ d and $(1.27 \pm 21.24)x^{(-0.083 \pm 2.036)}$ for $P_{\rm rot} \geq 55$ d

K-type stars: $(11.63 \pm 0.31)x^{(-0.43 \pm 0.005)}$ for $P_{\rm rot} < 40$ d and $(0.00 \pm 0.00)x^{(1.465 \pm 0.190)}$ for $P_{\rm rot} \geq 40$ d

G-type stars: $(3.73 \pm 0.10)x^{(-0.30 \pm 0.006)}$ for $P_{\rm rot} < 30$ d and $(0.00 \pm 0.00)x^{(0.885 \pm 0.106)}$ for $P_{\rm rot} \geq 30$ d

F-type stars: $(0.64 \pm 0.04)x^{(-0.17 \pm 0.017)}$ for $P_{\rm rot} < 25$ d and $(0.06 \pm 0.23)x^{(0.102 \pm 0.504)}$ for $P_{\rm rot} \geq 25$ d

These fits produce smaller reduced χ^2 values for all the stellar types with the exception of K-type stars: 14.81 for M-type stars, 1586 for K-type stars, 259.5 for G-type stars, and 97.65 for F-type stars. Although these values are smaller than those of a single power-law fit, they are still too large to be statistically significant, suggesting that other factors including each star's activity cycle may need to be considered.

5.3 Vertical binning

Since the raw unbinned data of the previous section did not show statistical significance for a particular power law, we considered what physical principle might justify binning the data. Each star in the sample likely has its own stellar activity cycle over which the brightness will vary. Thus all of the data points in our sample come from potentially different points in each star's activity cycle, adding uncertainty to the exact stellar variation over rotation period

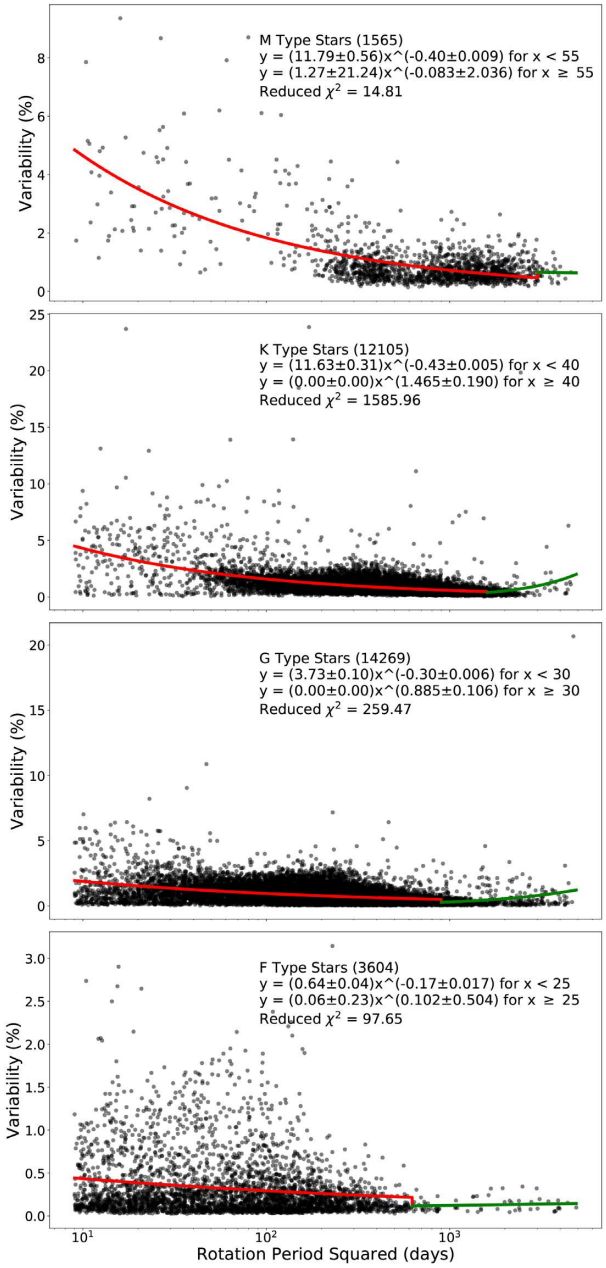

Figure 4. Variability versus rotation period squared with dual power-law fits for each stellar type split at the selected break period. The green line on each panel represents the fit for stars older than the given break period and the red line on each panel represents the fit for stars younger than the given break period. The particulars of the fits, along with the reduced χ^2 values are labelled on the plot for each stellar type.

squared. To account for this spread, we introduce vertical bins into our data, each with a constant width of 0.1 per cent variability based on empirical correlations between X-ray and bolometric variability (Preminger et al. 2011) as well as observed changes in the Sun's variability over its known activity cycle (Reinhold et al. 2017). We then fit the binned data with single and dual power laws as above, and assess evidence for multiple branches. We treat the mean of each bin as a single data point with a weight given by the fraction of stars in that stellar type in the bin.

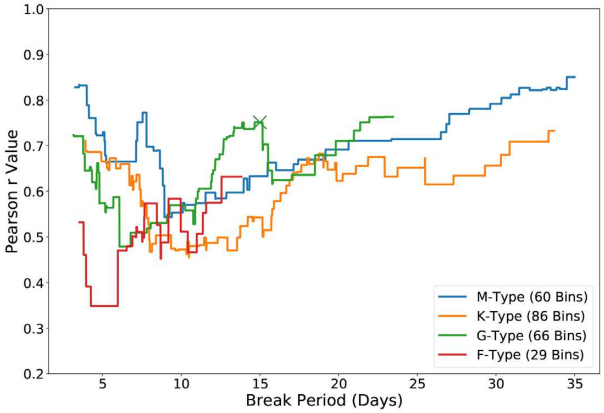

Figure 5. Pearson r values versus break period for the binned data of each stellar type, blue for M-type stars, orange for K-type stars, green for G-type stars, and red for F-type stars. As the only clear maximum in correlation occurs at 15 d for G-type stars (indicated with a green x), that is the only stellar type we fit with a dual power law. The number of bins for each stellar type is shown in the lower right corner.

5.3.1 *Single power law*

We fit our binned data with a single power law again using the LM minimization routine from Section 5.1. We find the best fits:

M-type stars: $(13.91 \pm 2.06)x^{(-0.30 \pm 0.037)}$, $\chi^2 = 3.19$
K-type stars: $(19.64 \pm 3.75)x^{(-0.31 \pm 0.044)}$, $\chi^2 = 3.71$
G-type stars: $(15.59 \pm 2.62)x^{(-0.36 \pm 0.045)}$, $\chi^2 = 4.28$
F-type stars: $(7.48 \pm 3.05)x^{(-0.43 \pm 0.113)}$, $\chi^2 = 1.54$

These fits of the binned data produce dramatically better reduced χ^2 values for both the single and dual power-law fits of the unbinned data. All of these values suggest that these fits are statistically significant.

5.3.2 *Dual power law*

To further compare our binned and unbinned results, we checked for any evidence of a dual power-law fit in the binned data. We again minimize equation (13) with our binned data and again find no clear statistically significant minima that would provide a break period choice to maximize the correlations, except possibly for G-type stars. Fig. 5 shows the weighted correlation coefficients for each stellar type as a function of the chosen break period. Only G-type stars show a maximum correlation that is not located at one of the edges of the possible break periods and therefore we only attempt a dual power-law fit for the binned data of G-type stars. The peak correlation of G-type stars corresponds to a break period of 15 d and from this we find the fits (shown in Fig. 6): $(15.11 \pm 2.75)x^{(-0.35 \pm 0.052)}$ and $(1.36 \times 10^8 \pm 9.79 \times 10^8)x^{(-3.18 \pm 1.31)}$ for stars with rotation periods lower and higher than 15 d, respectively. This dual power-law fit produces a lower reduced χ^2 value of 1.11, suggesting a higher statistical significance of a dual power-law fit than that of a single power law for the binned G-type stars.

5.3.3 *Branches*

The scatter in the binned data suggests another possible interpretation to test, namely the existence of multiple branches in the

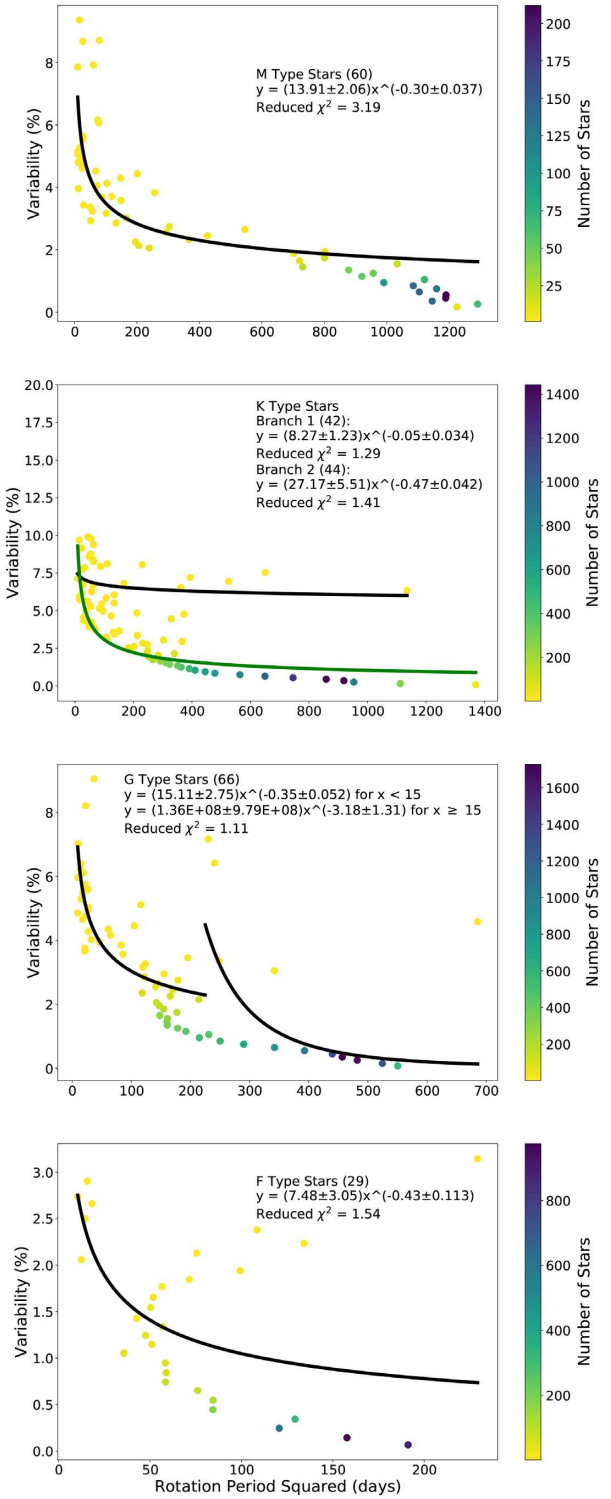

Figure 6. Variability versus rotation period squared with power-law fits for each stellar type where the sample has been split into vertical bins with a constant width of 0.1 per cent variability. The black line on the panels for M- and F-type stars represents the best fit found taking into account all bins which contain more than one star using an LM fitting routine, the black lines on the panel for G-type stars represent the fits for the bins with rotation periods less than and greater than 15 d and the black and green lines on the panel for the K-type stars represent the best fits for the two branches, above and below 4.45 per cent variability, using an LM fitting routine. The colour scale of each data point represents the number of stars in the bin represented by that point.

evolution of star-spot coverage with age. In particular, the binned data for K-type stars appears to have a structure that could be consistent with two separate branches rather than a single power law. We determine the two branches simply by grouping stars with variability above or below 4.45 per cent. This division is a visual cut for where there appear to be distinct branches. We find the best fits for K-type stars (shown in Fig. 6): $(8.27 \pm 1.23)x^{(-0.05 \pm 0.034)}$ and $(27.17 \pm 5.51)x^{(-0.47 \pm 0.042)}$ for the stars above and below 4.45 per cent variability, respectively.

From these fits, we find that two branches for the K-type stars produce smaller reduced chi-square values than a single fit of the binned data, 1.24 and 1.30 for K-type stars with variabilities above and below 4.45 per cent, indeed suggesting evidence for two branches of evolution for activity of K-type stars.

6 IMPLICATIONS FOR THE VALUE OF λ

Using equations (10) and (12), we are able to determine a value for λ for the single power-law fits of our binned data, as those are the fits with reduced χ^2 values indicating statistical significance. We find the values:

M-type stars: 0.222 ± 0.030
K-type stars: 0.233 ± 0.035
G-type stars: 0.265 ± 0.036
F-type stars: 0.316 ± 0.085

The dual power-law fit for the binned G-type stars also has a reduced χ^2 value indicating statistical significance, and we find the λ values

$P_{\rm rot} < 15$ d: 0.258 ± 0.040
$P_{\rm rot} \geq 15$ d: 2.356 ± 0.975

Additionally the two branches for the binned K-type stars have reduced χ^2 values indicating statistical significance, and we find the λ values:

$V < 4.45$ per cent 0.034 ± 0.025
$V \geq 4.45$ per cent 0.350 ± 0.036

All of the λ values we were able to determine are within the assumed range of $0 \leq \lambda \leq \frac{1}{3}$ from Blackman & Owen (2016), with the exception of the λ representing G-type stars with rotation periods greater than 15 d. The larger λ value for this subset of the sample provides some evidence for a flattening in the functional form of the evolution of star-spot coverage at a rotation period of 15 d for G-type stars. This period is different from that associated with a previously proposed weakening of magnetic braking at the solar age, corresponding to the 24.5 d rotation period (van Saders et al. 2016; Metcalfe & van Saders 2017). A weakening of magnetic braking through some kind of dynamo transition to higher multipoles could be related to the increase in λ: a higher λ means more sensitivity of star-spot coverage to X-ray luminosity. In turn, a reduction in magnetic braking for a given average magnetic field strength implies a higher fraction of smaller scale magnetic structures. Since it is these smaller structures which produce star-spots, we can speculate that λ could increase with a reduction in open field lines. In any case, more observational and theoretical work is needed for the 'first principles' understanding of λ from stellar dynamo theory, but the empirically determined value is of practical use for simple holistic modelling.

7 CONCLUSIONS

To investigate the star-spot coverage of main-sequence stars, we have used a sample of over 30 000 *Kepler* stars with previously measured activity and rotation periods covering M, G, K, and F spectral types. Using the Pearson correlation coefficient, we determined that there exists a decrease in star-spot coverage with increasing rotation period – a proxy for age – for each of these spectral types. We tried to describe this relationship in the unbinned raw data with single and dual power-law fits using an LM minimization routine, and found high reduced χ^2 values for each stellar type in both cases, although those of the dual power-law fits are somewhat smaller than those of the single power law for all types except for the K-type stars.

After introducing vertical bins to account for the variability within activity cycle periods of each individual star, we found much lower reduced χ^2 values than those of the unbinned data, indicating statistically significant fits for each stellar type. We found no evidence for power-law breaks in the binned data except for the G-type stars, in which a break occurs at a rotation period of 15 d. This dual power-law fit for G-type stars produced a lower reduced χ^2 value than the single power law. We also found evidence of two separate branches for the evolution of K-type stars, those above and below 4.45 per cent variability, which further decreases the reduced χ^2 values, indicating a higher statistical significance for these branches than a single power law. We compared fits using bin means and medians for all stellar types, and found the only significant difference to be somewhat reduced evidence for the two branches for the K-type stars.

From our fits, we determined values for the model parameter λ used in Blackman & Thomas (2015) to account for the decreasing evolution of star-spot coverage with age. We found values in concordance with their assumed range of $0 \leq \lambda \leq \frac{1}{3}$ for the single power-law fit for all stellar types. We also found concordance for both branches of K-type stars. For the dual power-law fit to G-type stars, we found concordance at rotation periods below 15 d. The λ value for G-type stars with rotation periods greater than 15 d is over 2σ outside the range of Blackman & Thomas (2015), indicating some evidence for a flattening in the functional form of the evolution of star-spot coverage. This piques further interest into a potential transition for G-type stars.

Although vertical binning was a practical step towards alleviating the influence of variability within each stars stellar cycle on the spread in the raw data, future work could improve upon this if large samples were to ever become available with known activity cycles, so that stars can be compared at the same phase in their cycles. Additionally, more observational and theoretical work is needed to understand the parameter λ from stellar dynamo theory.

ACKNOWLEDGEMENTS

We thank the referee for a helpful, meticulous report. EB acknowledges support from National Science Foundation Grant AST-1813298, Kavli Institute for Theoretical Physics (University of California Santa Barbara) funded by National Science Foundation Grant PHY-1748958, and Aspen Center for Physics funded by National Science Foundation Grant PHY-1607611.

REFERENCES

Baliunas S. L., Vaughan A. H., 1985, ARA&A, 23, 379
Baliunas S. L. et al., 1995, ApJ, 438, 269
Blackman E. G., Owen J. E., 2016, MNRAS, 458, 1548
Blackman E. G., Thomas J. H., 2015, MNRAS, 446, L51
Böhm-Vitense E., 2007, ApJ, 657, 486
Brandenburg A., Saar S. H., Turpin C. R., 1998, ApJ, 498, L51
Charbonneau P., 2014, ARA&A, 52, 251
Cranmer S. R., Saar S. H., 2011, ApJ, 741, 54
Dmitrienko E. S., Savanov I. S., 2017, Astron. Rep., 61, 122
do Nascimento J.-D., Jr., Saar S. H., Anthony F., in van Belle G., Harris H. C., eds, 2015, 18th Cambridge Workshop on Cool Stars, Stellar Systems, and the Sun, Vol. 18, Cambridge Workshop on Cool Stars, Stellar Systems, and the Sun Lowell Observatory, Flagstaff, Arizona
Domingo V. et al., 2009, Space Sci. Rev., 145, 337
Dressing C. D., Charbonneau D., 2013, ApJ, 767, 95
Drilling J. S., Landolt A. U., 2000, in Cox A. N., ed., Normal Stars, American Institute of Physics Press, Springer, New York, p. 381
Duvall T. L., Dziembowski W. A., Goode P. R., Gough D. O., Harvey J. W., Leibacher J. W., 1984, Nature, 310, 22
Hartmann L. W., Noyes R. W., 1987, ARA&A, 25, 271
Kraft R. P., 1967, ApJ, 150, 551
Mamajek E. E., Hillenbrand L. A., 2008, ApJ, 687, 1264
McQuillan A., Aigrain S., Mazeh T., 2013, MNRAS, 432, 1203
McQuillan A., Mazeh T., Aigrain S., 2014, ApJS, 211, 24
Messina S., Guinan E. F., 2002, A&A, 393, 225
Metcalfe T. S., van Saders J., 2017, Sol. Phys., 292, 126
Micela G., Sciortino S., Serio S., Vaiana G. S., Bookbinder J., Golub L., Harnden F. R., Jr., Rosner R., 1985, ApJ, 292, 172
Montesinos B., Thomas J. H., Ventura P., Mazzitelli I., 2001, MNRAS, 326, 877
Notsu Y. et al., 2019, ApJ, 876, 58
Noyes R. W., Hartmann L. W., Baliunas S. L., Duncan D. K., Vaughan A. H., 1984, ApJ, 279, 763
Noyes R. W., Weiss N. O., Vaughan A. H., 1984, ApJ, 287, 769
Oláh K., Strassmeier K. G., 2002, Astron. Nachr., 323, 361
Oláh K., Kolláth Z., Strassmeier K. G., 2000, A&A, 356, 643
Pallavicini R., Golub L., Rosner R., Vaiana G. S., Ayres T., Linsky J. L., 1981, ApJ, 248, 279
Parker E. N., 1955, ApJ, 122, 293
Petrovay K., van Driel-Gesztelyi L., 1997, Sol. Phys., 176, 249
Pizzolato N., Maggio A., Micela G., Sciortino S., Ventura P., 2003, A&A, 397, 147
Preminger D. G., Chapman G. A., Cookson A. M., 2011, ApJ, 739, L45
Randich S., 2000, in Pallavicini R., Micela G., Sciortino S., eds, ASP Conf. Ser. Vol. 198, Stellar Clusters and Associations: Convection, Rotation, and Dynamos. Astron. Soc. Pac., San Francisco, p. 401
Reiners A., Schüssler M., Passegger V. M., 2014, ApJ, 794, 144
Reinhold T., Cameron R. H., Gizon L., 2017, A&A, 603, A52
Saar S. H., Brandenburg A., 1999, ApJ, 524, 295
Savanov I. S., Dmitrienko E. S., 2017a, Astron. Rep., 61, 461
Savanov I. S., Dmitrienko E. S., 2017b, Astron. Rep., 61, 996
Savanov I. S., Dmitrienko E. S., 2018, Astron. Rep., 62, 238
Skumanich A., 1972, ApJ, 171, 565
van Saders J. L., Ceillier T., Metcalfe T. S., Silva Aguirre V., Pinsonneault M. H., García R. A., Mathur S., Davies G. R., 2016, Nature, 529, 181
Vaughan A. H., Preston G. W., 1980, PASP, 92, 385
Vaughan A. H., Preston G. W., Wilson O. C., 1978, PASP, 90, 267
Vidotto A. A. et al., 2014, MNRAS, 441, 2361
Vilhu O., 1984, A&A, 133, 117
Wilson O. C., 1966, ApJ, 144, 695
Wilson O. C., 1978, ApJ, 226, 379
Wright N. J., Drake J. J., Mamajek E. E., Henry G. W., 2011, ApJ, 743, 48

APPENDIX: COMPARISON OF MEDIANS AND MEANS OF BINNED DATA

To ensure that the trends in the binned data are not affected by the use of the mean values, we compare the trends seen in the medians of the bins with those seen in means of the bins as shown in Fig. A1.

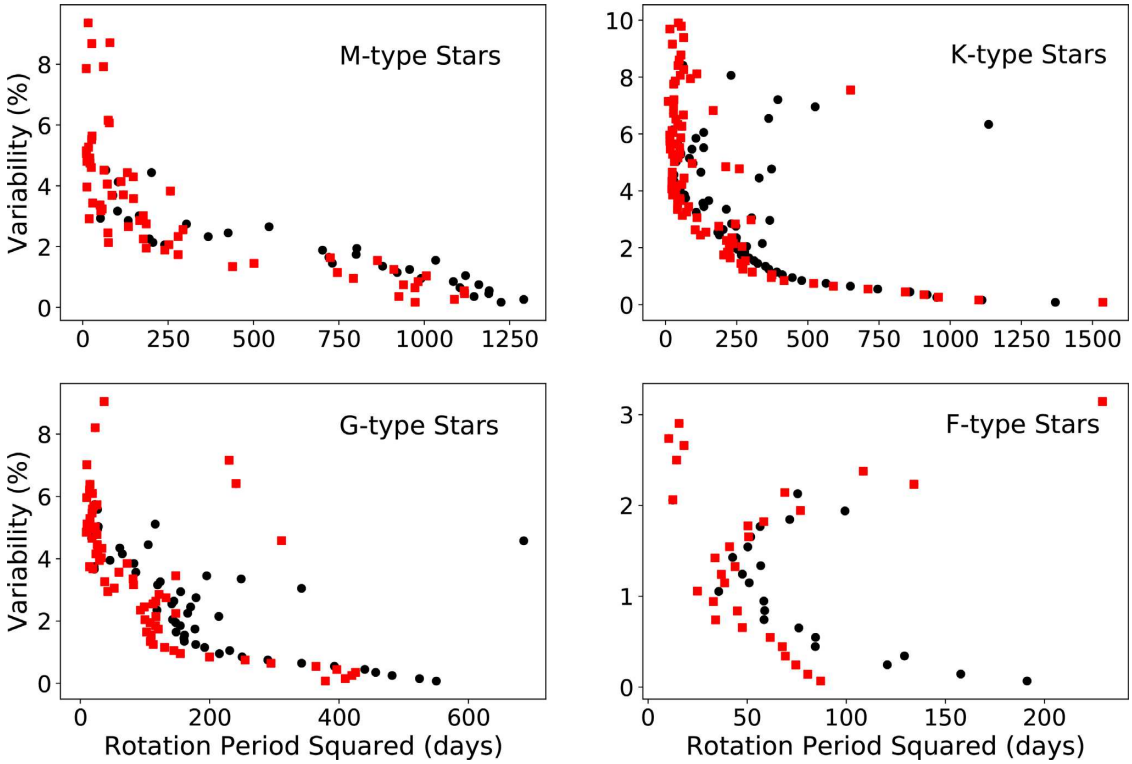

Figure A1. Comparisons of trends seen when using the medians versus the means of the rotation period squared and variability of the binned data for each stellar type. The black circles in each panel represent the means of the bins and the red squares represent the medians of the bins. In each case, the trends seen in the medians and means are the same with the exception of more evidence for a second branch in the means of K-type stars than in the medians.

We use the same bins in variability of constant width 0.1 per cent as in Section 5.3 and represent each bin with either the average or the median rotation period and variability. The same trends are seen in the medians and means for M-, G-, and F-type stars. For K-type stars, there appears to be more evidence for a second branch in the means of the bins than in the medians, but there does still exist some evidence for a second branch in the medians.

This paper has been typeset from a TEX/LATEX file prepared by the author.